(110)-Exposed Gold Nanocoral Electrode as Low Onset Potential Selective Glucose Sensor

Ta-Ming Cheng,[†] Ting-Kai Huang,[†] Huang-Kai Lin,[†] Sze-Ping Tung,[†] Yu-Liang Chen,[†] Chi-Young Lee,[‡] and Hsin-Tien Chiu*[,†]

Department of Applied Chemistry, National Chiao Tung University, Hsinchu, Taiwan, 30050, R. O. C, Department of Materials Science and Engineering and Center for Nanotechnology, Materials Science, and Microsystems, National Tsing Hua University, Hsinchu, Taiwan, 30043, R. O. C

ABSTRACT A straightforward electrochemical deposition process was developed to grow gold nanostructures, including nanocoral, nanothorn, branched belt, and nanoparticle, on carbon electrodes by reducing $HAuCl_4$ under constant potentials in mixtures containing CTAC and/or $NaNO_3$. Among the nanostructures, the quasi-one-dimensional nanocoral electrode showed the highest surface area. Because of this, it provided excellent electrochemical performances in cyclic voltammetric (CV) studies for kinetic-controlled enzyme-free glucose oxidation reactions. In amperometric studies carried out at 0.200 V in PBS (pH 7.40, 0.100 M), the nanocoral electrode showed the highest anodic current response. It also offered the greatest sensitivity, 22.6 $\mu AmM^{-1}cm^{-2}$, an extended linear range, 5.00×10^{-2} mM to 3.00×10^{1} mM, and a low detection limit, 1.00×10^{1} μm among the electrodes investigated in this study. In addition, the glucose oxidation by the nanocoral electrode started at −0.280 V, more negative than the one of using a commercial Au electrode as the working electrode. This is attributed to the presence of exposed Au (110) surfaces on the electrode. The feature was applied to oxidize glucose selectively in the presence of ascorbic acid (AA) and uric acid (UA), common interferences found in physiological analytes. With an applied voltage at −0.100 V, the AA oxidation (started at −0.080 V) can be avoided while the glucose oxidation still provides a significant response.

KEYWORDS: Au nanostrucre • Au (110) plane • selective oxidation • electrochemical glucose sensor

INTRODUCTION

Electrocatalytic glucose oxidation is an important research topic in several fields, such as employing glucose in ecologically friendly bio-fuel cells for next generation energy source and sensing glucose in blood for medical applications (1, 2). Owning increasing number of people suffering from diabetes recently, many scientists have paid a great deal of attention to the improvement of glucose sensors for blood sugar levels. Clark and Lyons reported the first glucose sensor based on an electrode modified with enzymes in 1962 (3). Glucose oxidase (GOD) has been a common enzyme for glucose oxidation in the presence of oxygen (4). It can catalyze glucose to gluconolactone and produce H_2O_2 as a byproduct. Glucose concentration can be estimated from the electrochemical response of the H_2O_2 concentration (5−10). In addition, this type of sensors have shown high selectivity to glucose in the analyte. Although these biosensors are widely used, their practical applications are limited by many problems. They suffer from intrinsic instability, complicated immobilization processes in fabrications, and oxygen concentrations in the environment (4, 11). Thus, sensors based on direct oxidation of glucose without using enzymes have been expected to avoid such problems.

There have been many reports related to applying Cu, Pt, and Au metals as the potential electrochemical electrodes (12−18). For Cu electrodes, an alkaline solution environment is frequently required for the experiments (18). Although Pt electrodes show high catalytic properties in neutral buffers, they are easily poisoned by intermediates and products generated in the experimental processes so that their intrinsic activities are suppressed (19). Although Au is more stable toward oxidation and poisoning during the experiments, high overpotential and poor sensitivity are always serious challenges for applying Au as an effective glucose sensor to oxidize glucose (20). Because of the high potential, interfering molecules in the analyte, such as ascorbic acid (AA), are easily oxidized. Consequently, signals from glucose and AA cannot be discriminated easily. Some strategies may be applied to solve this drawback in selectivity. From early research, it is well-known that electrodes with increased surface areas can provide improved performances for kinetically controlled reactions, such as glucose oxidation. On the other hand, it influences diffusion-controlled reactions, for example, AA oxidation, only slightly. Thus, fabricating electrodes with high surface areas is a promising method to increase electrochemical response of glucose but not the one of AA (15). Immobilization of metal nanoaprticles on supporting material such as carbon nanotubes and conductive molecules are frequently used to increase the surface areas (21, 22). In addition, hard templates are commonly employed to grow tubelike and porous metal electrodes (23−25). But these methods require complicated

* Corresponding author. E-mail: htchiu@faculty.nctu.edu.tw (H.-T.C.).
Received for review May 17, 2010 and accepted August 30, 2010
[†] National Chiao Tung University.
[‡] National Tsing Hua University.
DOI: 10.1021/am100432a

processing steps. Hence, a template-free method may simplify the fabrication of high surface area electrode significantly (26).

In addition to surface areas, chemical reaction kinetics is highly influenced by the nature of the electrode materials. For example, in a recent study, a Pt/Pd composite electrode was used to achieve a glucose oxidation voltage more negative than the one used for AA oxidation (27). Also, several studies show that surface reactions are strongly dependent on crystalline orientations (28, 29). This is because different crystal surfaces provide different adsorption sites for reactants, intermediates, and products. For instance, in glucose oxidation, the oxidative currents generated from Au (111) and Au (100) planes were higher than the one produced from Au (110) plane. On the other hand, the onset potential observed for the glucose oxidation on Au (110) was much lower than the ones found for that on Au (111) and Au (100) (28). Therefore, we anticipate that by oxidizing glucose on Au(110) at a low potential, interfering signals from the oxidations of other molecules may be avoided. As a result, fabrication of a high-surface-area Au electrode with exposed (110) planes as an enzyme-free glucose sensor appears to be an interesting challenge.

Previously, we reported the growths of several one-dimensional nanostructured metals, including Cu and Ag nanobelts, Au nanowires and Cu nanorods, directly on substrates via simple galvanic reductions (30−32). The morphologies of the as-grown products were highly influenced by the growth conditions, including the surfactant and the anion concentrations, and the reaction temperatures. In this study, we deposit Au nanostructures on commercial carbon screen printed electrodes via a simple electrodeposition route. Using this method, the applied currents can be quantified. Therefore, the amounts of Au deposited on the substrates can be estimated. We are able to fabricate several Au electrodes with different morphologies, including nanocoral, branched belt, nanothorn, and nanoparticle. Among them, the nanocoral electrode not only provides high surface areas but also Au (110)-like properties toward glucose oxidation. In phosphate buffer solutions (PBS), it demonstrates a great sensitivity, an extended linear range, and selectivity for glucose oxidation. Our discoveries are discussed below.

EXPERIMENTAL SECTION

Reagents. Gold chloride trihydrate (Aldrich), cetyltrimethylammonium chloride (CTAC, Taiwan surfactant), sodium nitrate (Aldrich), sodium phosphate dibasic dihydrate (Aldrich), sodium phosphate monobasic monohydrate (JT-Baker), D-(+)-glucose (Aldrich), L-ascorbic acid (AA, Aldrich), and uric acid (UA, Aldrich) were used without further purification.

Preparation of Electrodes.

Nanocoral Electrode. A process similar to the fabrication of one-dimensional Au nanowires was employed here (28). When a CTAC solution (8.90×10^1 mM, 0.500 mL) was added to a $HAuCl_4$ solution (5.00×10^1 mM, 0.500 mL), the mixture turned from transparent yellow to a suspension of yellow colloids. Then, $NaNO_3$ (1.00×10^2 mM, 1.00 mL) and deionized water (3.00 mL) were assed so that the final suspension contained 5.00 mM $HAuCl_4$, 8.90 mM CTAC, and 2.00×10^1 mM $NaNO_3$. After this mixture was sonicated for 5 min, it was placed in a water bath at 290 K. Electrochemical reduction was performed using a two-electrode electrochemical cell composed of a DC power supply and two carbon electrodes. The cathode was a carbon screen printed electrode, purchased from Zensor R&D with a geometric area of 0.196 cm^2. The anode was fabricated by painting carbon paste on a transparent projection slide and dried at 343 K on a hot plate under air. Prior to the electrochemical process, the electrodes were rinsed by deionized water and dried by a stream of N_2 gas. After the electrodes were immersed into the colloidal suspension, a voltage fixed at 1.80 V was supplied at 290 K for 18 h. The total charge supplied to the cell was quantified to be 0.20 C. Formation of a dark-red surface on the screen printed carbon electrode (the cathode) was observed (total Au deposited: 0.69 μmol, 140 μg). Finally, the as prepared electrode was rinsed by using deionized water and stored under air before further use.

Other Electrodes. Procedures employing growth parameters varied from the ones discussed above were employed for the preparation of other electrodes with different morphologies. All reactions were performed at 290 K with a total supplied charge of 0.20 C. Branched belt electrode was fabricated by using an electrolyte containing $HAuCl_4$ (5.00 mM), CTAC (8.90 mM), and $NaNO_3$ (2.00×10^1 mM) as the electrolyte at an applied voltage 1.60 V in 24 h. For Au nanothorn electrode, $HAuCl_4$ (5.00 mM) mixed with $NaNO_3$ (2.00×10^1 mM) was reduced at 1.80 V. Because the electrolyte did not contain CTAC, the reaction was completed after 25 min. The third type of electrode, nanoparticle electrode, was grown at 1.80 V using an electrolyte composed of $HAuCl_4$ (5.00 mM) and CTAC (8.90 mM). The overall reduction time was 20 h. A summary of the electrochemical reaction conditions is shown in Table S1 in the Supporting Information.

Electrochemical properties of the electrodes prepared in this study were compared to the flat Au electrodes (geometric area 0.196 cm^2) purchased from Zensor R&D.

Instrumentation. The electrodes fabricated in this study were characterized by scanning electron microscopy (SEM, JEOL JSM-7410F at 15 kV), transmission electron microscopy (TEM, JEOL JEM-4000EX), electron diffraction (ED, using LaB_6 as the electron source, accelerated at 400 keV), and X-ray diffraction, (XRD, Bruker AXS D8 Advance). Cyclic voltammetric (CV) and amperometric experiments were carried out on a CHI 6081C (CH Instruments) electrochemical analyzer. A three-electrode system was employed for the measurements. It contained a working electrode, which is an Au electrode fabricated in this study, a counter electrode composed of a Pt wire, and an Ag/AgCl (in 3.00M KCl) reference electrode, with a potential of 0.200 V vs. standard hydrogen electrodes (SHE).

RESULTS AND DISCUSSION

Preparation and Characterization of Au Nanostructures. A process similar to the fabrication of one-dimensional Au nanowires was employed to fabricate the nanostructured Au electrodes (31). In general, electrochemical reduction of an electrolyte containing $HAuCl_4$ mixed with CTAC and/or $NaNO_3$ was carried out using a two-electrode cell system composed of carbon electrodes. A fixed DC voltage was applied for a period of a time so that a total charge of 0.20 C was supplied to grow 140 μg of Au on the cathode. Four types of electrodes, composed of nanocoral, branched belt, nanothorn, and nanoparticle, were fabricated. A summary of the reaction conditions is listed in Table S1 in the Supporting Information. Electrochemical properties of the fabricated electrodes were compared to the flat Au electrodes supplied by Zensor R&D. Because the nanocoral

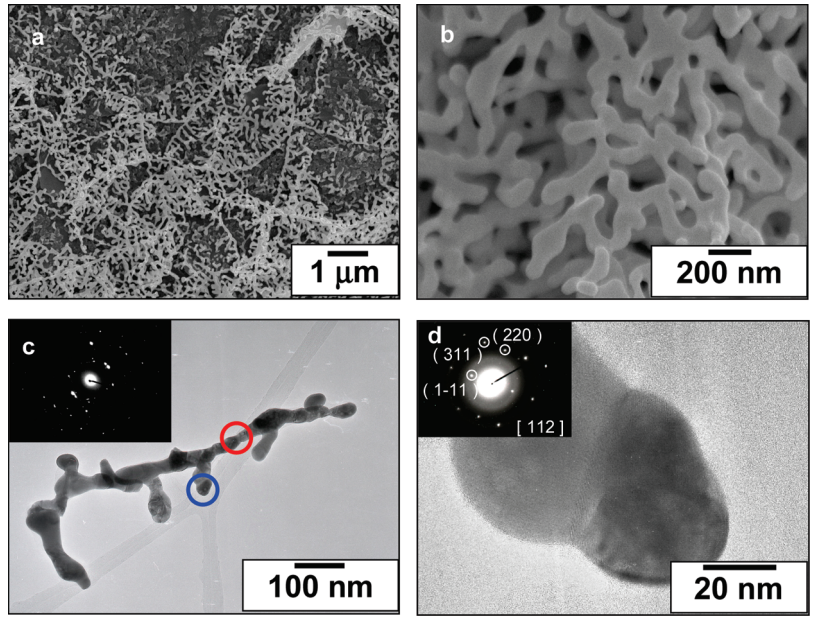

FIGURE 1. (a) Low- and (b) high-magnification SEM images of nanocoral electrodes. (c) Low-magnification TEM image (inset, SAED from the red circle) and (d) high-magnification TEM image from the blue circle in c (inset, SAED).

showed the best performance among them, its characterization will be discussed in detail below.

As shown in Figure 1a, a low-magnification SEM image displays that the surface of an as-deposited electrode is densely covered by coral-like quasi-one-dimensional nanostructures. The high magnification image shown in Figure 1b suggests that the widths of the coral structures are about 100−200 nm. In Figure 1c, a low-magnification TEM image of a nanocoral, with a major stem and several branches, is presented. Each branch has a width about 100 nm. This agrees well with the SEM result. The clear contrasts from different areas of this nanostructure indicate that the nancoral is composed of many grains. This is confirmed by the selected area electron diffraction (SAED) pattern (inset, Figure 1c) from the red circled area shown in Figure 1c. The pattern suggests the presence of a polycrystalline structure. A high magnification image from the blue circle is shown in Figure 1d. The SAED pattern in the inset shows the dot pattern of a single crystal. From both SAED patterns, the d spacings are estimated. They are consistent with the reflections from corresponding Au planes. In addition, the crystallographic zone axis is determined to be [112]. From the electrochemical characterizations discussed below, we discover that the surface structure of the nanocoral resembles that of the branched belt, with highly exposed Au(110) planes.

XRD were used to analyze the crystal structure of the electrodes prepared in this study also. In the Supporting Information, Figure S1 showed the XRD pattern of a nanocoral electrode. The peaks at 2θ = 38.1°, 44.3°, 64.5°, 77.5°, and 81.7 were assigned to Au (111), (200), (220), (311), and (222) reflections, respectively (JCPDF 89-3697). In addition, the peaks from the carbon electrode substrate were observed at 2θ = 46.3, 54.4, and 86.8°. The XRD result confirmed that face-centered-cubic (FCC) Au is a major component on the electrode.

Characterization data of other electrodes are shown in the Supporting Information. In Figure S2, SEM images of nanoparticle, nanothorn, and branched belt electrodes were presented. They all showed XRD patterns similar to the one displayed in Figure S1 in the Supporting Information. A sample from the branched belt electrode was further investigated by TEM, as shown in Figure S3 in the Supporting Information. The image in Figure S3a in the Supporting Information displayed many ripplelike patterns. This feature, originated from the strains of bending of thin samples, was frequently observed in TEM studies for nanobelts (30). In addition, a boundary region near the middle of the sample was observed. The SAED of this region, from the red circle in Figure S3a, showed a superposition of two identical patterns with a twisted angle of 70.53°. Each pattern was composed of dots from (111) and (200) planes while [110] was determined to be the zone axis. As a consequence, we conclude that the branched belt surface was an exposed Au (110) plane. This is further confirmed by the electrochemical characterization of the electrode discussed below.

Surface Area Determination. Because all of the electrodes grown in this study contained the same amount of Au, their real surface areas (RSA) were characterized by CV in a 0.5 M H_2SO_4 solution. The corresponding CV diagrams are shown in Figure 2. The anodic responses starting at 1.10 V are due to the formation of Au oxides (33). Subsequently, in the negative potential scan, they are reduced at about 0.900 V. By integrating the charge consumed for reducing the Au oxides formed in the positive scan, the RSAs of the electrodes are calculated by assuming that the reduction of a monolayer of Au oxides require 386 μC cm^{-2} (33). The results are listed in Table 1. Among all samples, the nanocoral electrode shows the highest RSA, 1.81 cm^2, whereas the commercial Au electrode has the lowest value, 0.155 cm^2. We suggest that the morphology and the exposed

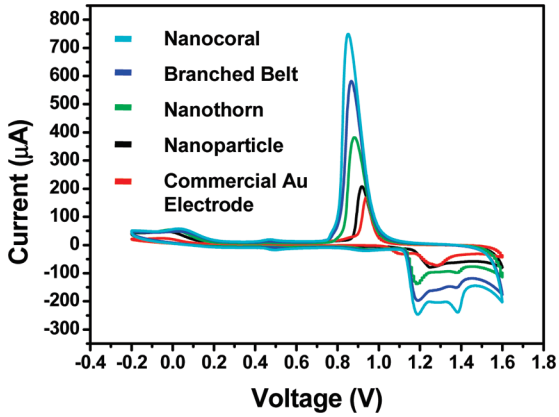

FIGURE 2. CV (100 mV/s) diagrams of Au electrodes in H_2SO_4 (0.5 M). The working electrodes are nanocoral (light blue), branched belt (blue), nanothorn (green), nanoparticle (black), and commercial (red) electrodes.

Table 1. Real Surface Areas (RSA) of Various Au Electrodes (geometric area: 0.196 cm^2) and Their Catalytic Properties for Glucose Oxidation Ability at 0.20 V in PBS (pH 7.40, 0.100 M)

	real surface area		glucose oxidation	
electrode	integrated coulomb (μC)	estimated RSA (cm^2)	sensitivity (μAcm^{-2} mM^{-1})	linear range (mM)
nanocoral	698.1	1.81	22.6	0.0500−30.0
branched belt	359.5	0.931	11.9	0.0500−40.0
nanothorn	230.0	0.596	6.4	0.0500−40.0
nanoparticle	101.2	0.262	2.00×10^{-2}	0.350−27.0
commercial electrode	60.00	0.155	5.00×10^{-3}	0.450−27.0

crystal planes are important factors to affect the RSAs. Electrodes with high RSAs are suitable for kinetically controlled reactions, such as glucose oxidation. Our observations are discussed below.

Electrocatalytic Oxidation of Glucose by Au Electrodes.

Cyclic Voltammetric Studies. The CV performance of the nanocoral Au electrode in the presence of 3.00 mM glucose is shown in Figure 3a. Based on previous literature reports, the CV scan is analyzed to rationalize the glucose oxidation process (28). In the blank scan, the curve displays reversible peaks at 0.280 V and 0.300 V. These can be assigned to OH adsorption to and desorption from the Au surface. During the negative scan, a current increase at 0.100 V is assigned to oxygen reduction in the solution. When glucose is added, the anodic current increases significantly. During the positive scan, the increase in the anodic current starts at approximately −0.280 V. This is marked as the onset of glucose oxidation. In addition, a broad anodic signal composed of two overlapping peaks at about 0.050 and 0.300 V is the result of a complicated process of glucose to gluconolactone oxidation (28). In the process, the first step is the formation of surface AuOH species. The oxidation of glucose is assumed to be through the interaction of surface AuOH groups and hemiacetal groups on glucose molecules nearby. Each one of the molecules releases two electrons to the Au electrode and oxidizes to gluconolactone. Then, the as-formed gluconolactone is hydrolyzed to produce

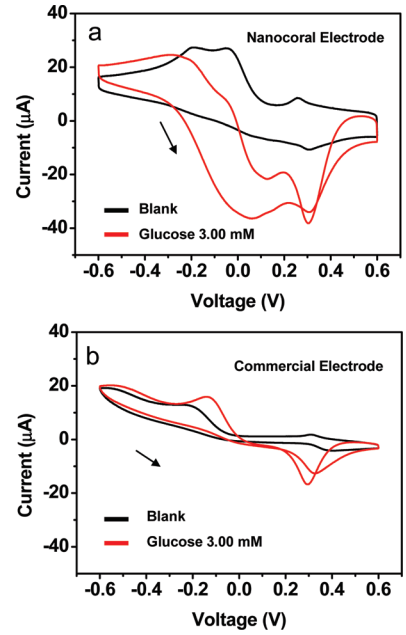

FIGURE 3. Comparison of CV scans before (black) and after (red) addition of glucose (3.00 mM) in PBS (pH 7.40, 0.100 M). The working electrodes are (a) nanocoral and (b) commercial Au electrodes.

gluconic acid. The observed electrochemical behavior is comparable to the reported performance of Au (110) surface toward glucose oxidation in PBS (28). Above 0.300 V, the anodic current decreases sharply because of the oxide formation on the Au surface. This suppresses further glucose oxidation near the electrode. In the negative scan, AuOH sites are formed again as the surface oxides are reduced. Therefore, the anodic current increases sharply, which can be ascribed to the reformation of active surface sites. This signal is very close to the one observed for the oxide reduction on Au(111) surface (28). As a result, we suggest that some Au(111) surfaces are exposed on the nanocoral also. Because the signal are broad, contributions from a few exposed Au(100) planes cannot be ruled out. For comparison, the CV curves of a commercial Au electrode are displayed in Figure 3b. It presents weaker current responses than the nanocoral electrode does. This is understandable because the nanocoral Au electrode reported here has a much higher surface area than the commercial electrode does. Also, it shows a more positive onset potential, observed at −0.044 V, for glucose oxidation. The result resembles the one reported for an Au (111) electrode, suggesting that (111) planes are the major exposed surfaces (28). In the Supporting Information, Figure S4 shows the CV diagrams of the other electrodes prepared in this study. The CV curve of the branched belt electrode (Figure S4a) was similar to the one of the nanocoral electrode. The overall glucose oxidation performance of the branched belt electrode resembled that of the Au (110) electrode also. The observation is consistent with the TEM result, which showed that the exposed surface of the branched belt was Au (110). Panels b and c in Figure S4 in the Supporting Information reveal the CV diagrams of the nanothorn and the nanoparticle electrodes. Both are similar to the data of the nanocoral and the branched belt electrodes discussed above, suggest-

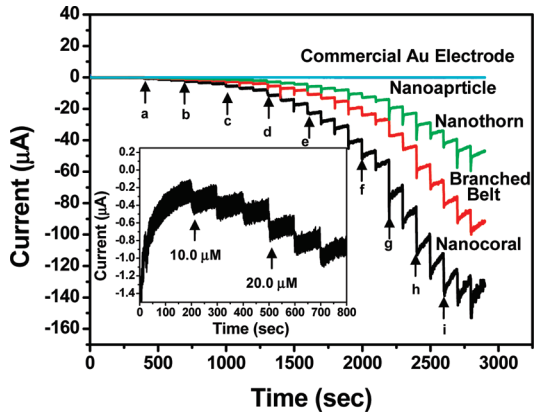

FIGURE 4. Amperometric current responses at 0.200 V. Glucose was successively injected ((a) 5.00×10^{-2} mM, (b) 1.00×10^{-1} mM, (c) 2.00×10^{-1} mM, (d) 5.00×10^{-1} mM, (e) 1.00 mM, (f) 2.00 mM, (g) 5.00 mM, (h) 8.00 mM, and (i) 10.00 mM) into stirred PBS (pH 7.40, 0.100 M). The working electrodes are nanocoral (black), branched belt (red), and nanothorn (light green). Responses from nanoparticle (blue) and commercial (light blue) Au electrodes are too weak to be seen clearly. Inset shows the lowest concentration to be detected at 1.00×10^{1} μM.

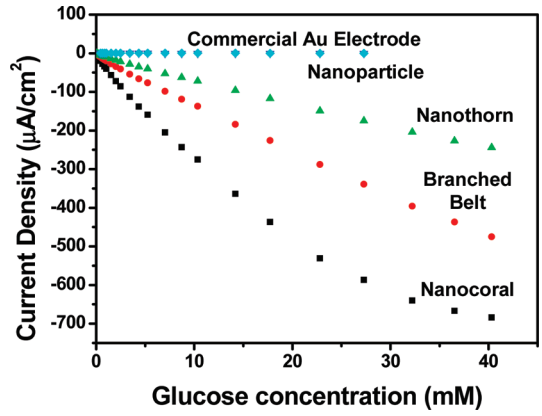

FIGURE 5. Calibration curves of amperometric tests shown in Figure 4. The working electrodes are nanocoral (black), branched belt (red), and nanothorn (light green). Responses of nanoparticle (blue) and commercial (light blue) Au electrodes are too weak to be seen clearly.

ing that their (110) surfaces were highly exposed too. The nanoparticle electrode showed the lowest current response. This is attributed to its relatively low surface area and poor adsorption of hydroxides from the solution. We discovered that while the RSA of the nanocoral electrode is about twelve times higher than that of the commercial electrode (Table 1), the anodic current of the nanocoral is only twice of the commercial one (Figure 3). This is another support that the nanocoral electrode has highly exposed Au (110) surfaces. According to the literature, with the same surface areas, the Au (110) surface provided a smaller anodic current than did the Au (111) and the Au (100) (28).

Amperometric Studies. In theory, the amperometric current should respond linearly to the glucose concentration at a fixed voltage. Thus, the catalytic glucose oxidation capabilities of the electrodes can be evaluated. In order to fit the physiology condition, we employed a PBS solution (pH 7.40, 0.100 M) as our electrolyte. Also, to prevent oxidation of the Au electrode surfaces that may suppress glucose oxidation during the amperometric tests and to avoid strong background currents, a constant potential at 0.200 V was selected for the studies. Glucose with known concentration was then injected sequentially into the electrolyte at an interval of 100 s. The results are shown in Figure 4. It indicates that the nanocoral electrode performs the best. A rapid increase in the anodic current can be observed after each addition of glucose to the stirred solution. The inset in Figure 4 shows that the detection limit is 1.00×10^{1} μM of glucose. The branched belt and the nanothorn electrodes respond less to the glucose additions. On the other hand, the nanoparticle and the commercial Au electrodes performed poorly, as shown in Figure S5 in the Supporting Information. This can be reasoned by their low surface areas. In Figure 5, the calibration curves derived from the data shown in Figure 4 are shown. An extended linear range from 5.00×10^{-2} mM to 3.00×10^{1} mM is shown for the nanocoral electrode. The result suggests that the electrode is potentially suitable for the physiological glucose concentration (3 − 8 mM) (34). The nanocoral electrode also possesses the highest calculated sensitivity among all electrodes investigated in this study, 22.6 μA cm^{-2} mM^{-1}. The linear range and the sensitivity of the other electrodes are summarized in Table 1. For comparison, we have listed some results from other Au and Pt glucose sensors in Table 2.

Selectivity of Nanocoral Electrode. In real physiological samples, AA and UA with concentrations about one-tenth of the glucose value normally coexist with it. Their presence may interfere with the electrochemical detection of glucose. To investigate whether the nanocoral electrode fabricated in this study may selectively detect glucose in the presence of AA and UA, we performed the following investigations. The CV scans of the electrode in 3.00 mM glucose, 3.00 mM AA, and 3.00 mM UA are shown in Figure 6a. There is no apparent response from UA. On the other hand, AA is easily oxidized above −0.080 V, the onset potential, and shows a great response that overwhelms the signal generated from the glucose oxidation.Because of the exposed Au (110) surface of the nanocoral electrode, the onset potential for the glucose oxidation is observed at −0.280 V, which is much lower than the one recorded for the AA oxidation. Thus, a relatively strong anodic response from the glucose oxidation can still be seen between −0.280 and −0.080 V in Figure 6a. The CV scans of the commercial Au electrode are shown in Figure 6b. Because of its smaller surface area, all of the responses are weaker than the ones obtained from the nanocoral electrode. In addition, the anodic response of the glucose oxidation, because of its higher onset potential, is completely surpassed by the AA oxidation signal. The amperometric responses of glucose (10.0 mM) and AA (1.00 mM) oxidations in PBS between −0.100 and 0.200 V were further investigated. The results are shown in Figure 7. The data of the nanocoral electrode (Figure 7a) clearly indicates that the AA oxidation current at −0.100 V can be ignored in comparison with the glucose oxidation signal. On the other hand, by using the commercial Au electrode, AA oxidation is predominant within the applied potential range. There is

Table 2. Summary of Performances of Noble Metal Glucose Sensors

electrode	applied potential (V)	sensitivity (μA cm^{-2} mM^{-1})	linear range (mM)	detection limit (μM)	ref
Au nanocoral	0.200[a]	22.6	0.0500−30.0	10	this study
Au branched belt	0.200[a]	11.9	0.0500−40.0	10	this study
Au NPs/MPTS	0.16[a]	179	0−8	0.05	(22)
porous Au	0.25[a]	32	0−10	2	(35)
macroporous Au	0.35[b]	11.8	2−10	0.05	(25)
roughened Au	0.3[b]	N/A	0−57.5	0.75	(26)
Au nanotube array	0.25[b]	1.13	1−42.5	10	(24)
macroporous Pt	0.5[b]	31.3	0.001−10	0.1	(14)
mesoporous Pt	0.4[a]	9.6	0−10	N/A	(15)
Pt nanotube	0.4[b]	0.1	2−14	1	(16)
nanoporous Pt	0.4[a]	291.0	0−10	N/A	(17)
nanoporous Pt−Pb (50%) Network	0.4[a]	10.8	1−16	N/A	(27)
ACCU-CHECK comfort curve[c]	N/A	N/A	0.6−33.3	600	(36)
Au NPs/MWCT/Nafion[d]	0.3[a]	0.4	0.05−20	20	(37)
Pt NPs/SWCNT[d]	0.55[a]	2.11	0.5−5	0.5	(38)

[a] The reference electrode is an Ag/AgCl (in KCl 3.00 M) electrode (0.200 V versus SHE). [b] The reference electrode is a saturated calomel electrode (SCE) (0.242 V versus SHE). [c] The test strip is modified by glucose dehydrogenase. [d] The working electrode is modified by GOD.

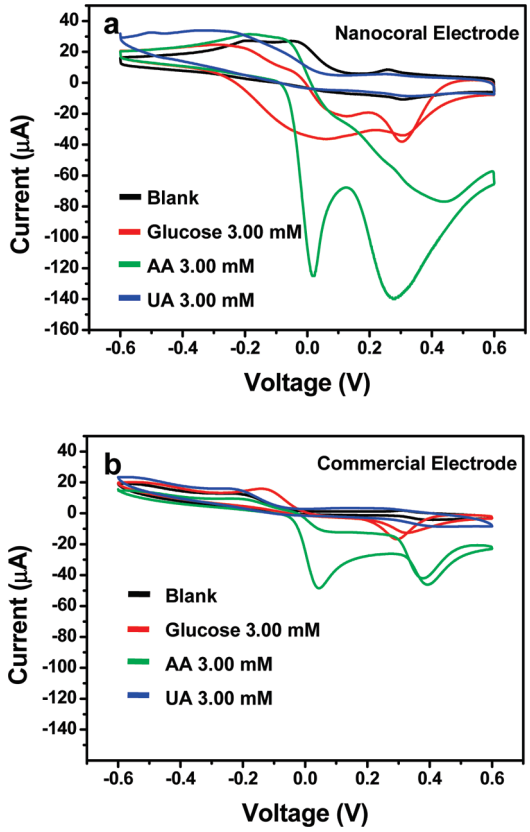

FIGURE 6. Comparison of CV scans. Blank (black), additions of glucose (3.00 mM, red), AA (3.00 mM, light green), and UA (3.00 mM, blue) in PBS (pH 7.49, 0.100 M) to (a) nanocoral and (b) commercial Au electrodes.

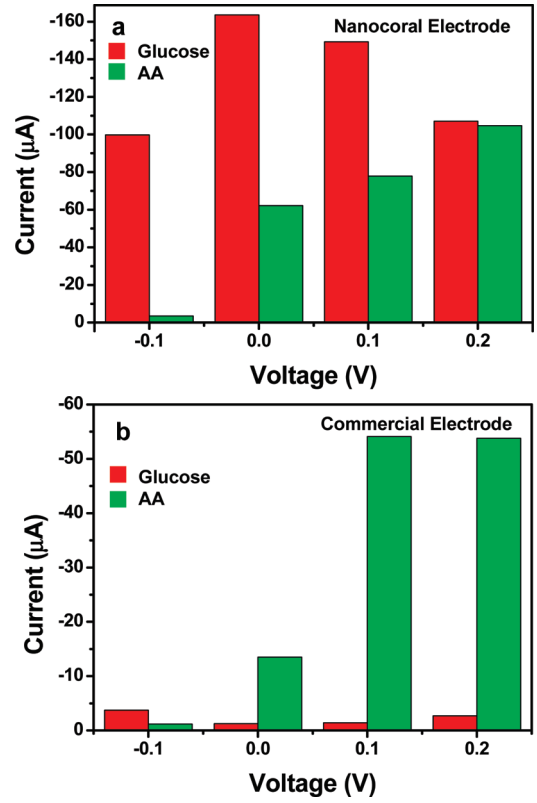

FIGURE 7. Comparison of amperometric signals of glucose (1.00×10^1 mM, red) and AA (1.00 mM, green) on (a) nanocoral and (b) commercial Au electrodes at different applied voltages in PBS (pH 7.40, 0.100 M).

no suitable potential to initiate an observable glucose oxidation reaction. As shown in Figure 8, analyses of interferences from AA and UA to glucose oxidation on the nanocoral electrode were performed at −0.100 V. Injecting UA (1.00 mM) to a PBS electrolyte (Figure 8a) does not generate a significant response. A clear signal is then observed after the addition of glucose (10.0 mM). A similar phenomenon is detected in Figure 8b for the introduction of AA (1.00 mM) followed by the addition of glucose. Figure 8c clearly shows that successive addition of AA and UA does not generate anodic signals. Further injection of glucose to the electrode still shows a clear oxidation signal. The glucose oxidation currents generated in the presence of UA (Figure 8a,c) are lower than the one produced without the addition of UA (Figure 8b). We suggest that although UA molecules are not oxidized, they may cap the Au surface sites so that the glucose oxidation ability is decreased. We believe the per-

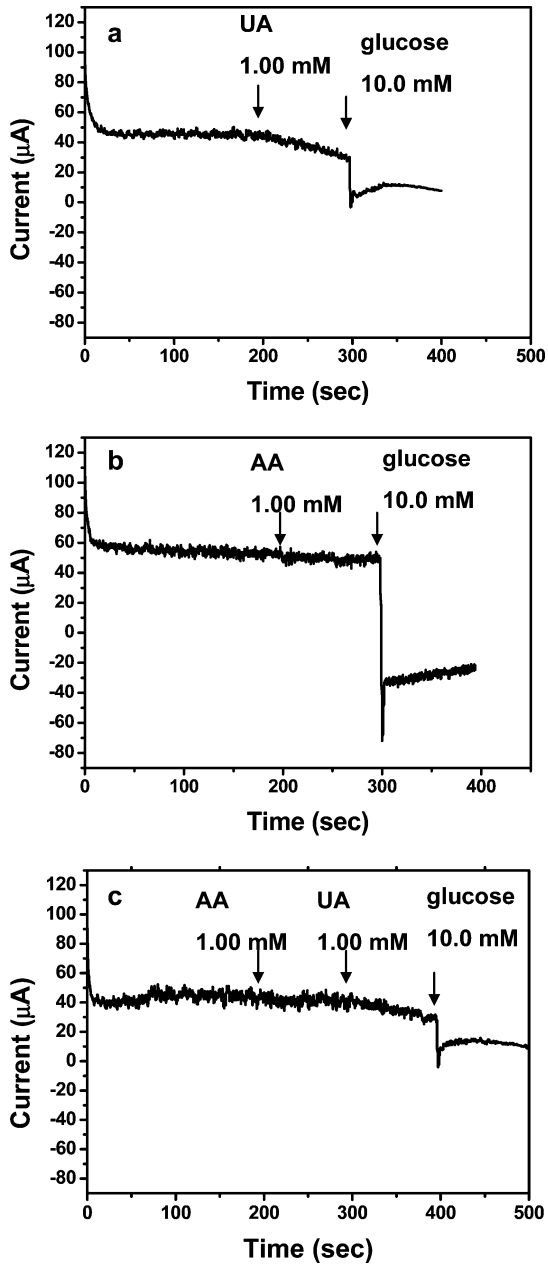

FIGURE 8. Interference analyses by amperometry at −0.100 V. The injection sequences are (a) UA (1.00 mM) and glucose (1.00×10^1 mM), (b) AA (1.00 mM) and glucose (1.00×10^1 mM), and (c) AA (1.00 mM), UA (1.00 mM) and glucose (1.00×10^1 mM).

formance of the nanocoral electrode can be improved by adjusting the electrode growth condition, the morphology, the real surface area, and the geometric area.

Stability of Nanocoral Electrode. The same nanocoral electrode was used repeatedly to oxidize glucose (1.00×10^1 mM) at 0.20 V for eight times. Between each measurement, deionized water was used to rinse the electrode surface and ten CV scan cycles were employed at a potential range from −1.00 V to 1.30 V in PBS (pH 7.40, 0.100 M). As shown in Figure S6 in the Supporting Information, no obvious anodic current decay can be observed. After these tests, the SEM image of the electrode was displayed in Figure S7 in the Supporting Information. The image indicated that the original nanocoral morphology was maintained. The data suggest that the electrode is stable upon repeated uses and cleanings. It is possible that fresh Au (110) surface is exposed again after the proper electrochemical process.

Comparison with Enzyme-Based Electrodes. To further evaluate the potential of our nanocoral electrode, we listed the performances of some enzyme-based glucose sensors in Table 2 (36−38). ACCU-CHEK Comfort Curve, a commercial test strip modified with potassium ferricyanide and glucose dehydrogenase on a substrate with supported Pd, has a similar measurement range, 0.6 − 33.3 mM (34). Its reported detection limit, 0.6 mM, is higher than that of our nanocoral electrode. We should be aware that the data of ACCU-CHEK Comfort Curve were taken in real physiological samples instead of PBS solutions. When the commercial strip is used to detect glucose concentration in blood, it has limited tolerance towards the interfering species, such as UA. When the UA concentration exceeds the limitation, it may cause deviation of response to glucose oxidation. Our nanocoral electrode also displays comparable tolerance towards the interfering species. It shows in Figure 8 a discernible signal at −0.100 V for 10 mM glucose in the presence of 1 mM UA and 1 mM AA. Our Au nanocoral electrode is further compared with some GOD-based CNT electrodes listed in Table 2. Although their detection limits are comparable, the sensitivity and the linear range of our electrode exceeds the performance of the GOD modified Au NPs/MWCNT/Nafion and Pt NPs/SWCNT electrodes (37, 38). Consequently, we anticipate that our Au nanocoral electrode will have a great potential for sensing glucose concentrations in physiological samples. Further investigations are in progress.

CONCLUSION

In this study, a simple electrochemical deposition method has been developed to grow gold nanostructures on commercial carbon electrodes. Different morphology, including nanocoral, branched belt, nanothorn, and nanoparticle, can be grown successfully. Among the electrodes fabricated, the nanocoral electrode shows the highest real surface area. This is the major reason why it provides the greatest sensitivity toward a kinetic-controlled glucose oxidation. By using the nanocoral electrode, the sensitivity for glucose oxidation is estimated to be 22.6 μA mM^{-1} cm^{-2} from 5.00×10^{-2} mM to 3.00×10^1 mM at an applied potential 0.200 V in PBS, whereas the detection limit is observed at 1.00×10^1 μm. Another important feature of the electrode is that it can oxidize glucose at a more negative on set potential than a common commercial Au electrode does. This is attributed to the presence of exposed Au (110) planes on the electrode surface. Because of this property, glucose in a mixture of glucose and AA can be selectively oxidized at −0.100 V. Thus, the interfering signal from AA oxidation can be excluded successfully. When the electrode is operated in a mixture of glucose, AA and UA, it can still provide a meaningful glucose oxidation signal response. We believe the electrochemical performance of the electrode can be improved further by optimizing the growth condition, the morphology, the real surface area, and the geometric area. Moreover, the electrode can be used repeatedly after a

proper cleaning procedure. All these properties suggest that the nanocoral electrode is a candidate for a promising glucose biosensor.

Acknowledgment. We are grateful for the support from the National Science Council, "Aim for the Top University Plan" of the National Chiao Tung University, and the Ministry of Education of Taiwan, the Republic of China. The authors thank Professor Y.-Z. Hsieh for discussion and help in electrochemical experiments.

Supporting Information Available: Summary of growth conditions of electrodes, XRD, SEM, TEM, ED, CV, and amperometric analyses data (PDF). This material is available free of charge via the Internet at http://pubs.acs.org.

REFERENCES AND NOTES

(1) Reach, G.; Wilson, G. S. *Anal. Chem.* **2008**, *64*, 381A.
(2) Kendall, K. *Nat. Mater.* **2002**, *1*, 211.
(3) Leland, C. C., Jr.; Champ, L. *Ann. N. Y. Acad. Sci.* **1962**, *102*, 29.
(4) Wilson, R.; Turner, A. P. F. *Biosens. Bioelectron.* **1992**, *7*, 165.
(5) Battaglini, F.; Bartlett, P. N.; Wang, J. H. *Anal. Chem.* **1999**, *72*, 502.
(6) Wilson, G. S.; Hu, Y. *Chem. Rev.* **2000**, *100*, 2693.
(7) Heller, A. *Acc. Chem. Res.* **2002**, *23*, 128.
(8) Zen, J.-M.; Kumar, A. S.; Chung, C.-R. *Anal. Chem.* **2003**, *75*, 2703.
(9) Lawrence, N. S.; Deo, R. P.; Wang, J. *Anal. Chem.* **2004**, *76*, 3735.
(10) Mano, N.; Heller, A. *Anal. Chem.* **2005**, *77*, 729.
(11) Park, S.; Boo, H.; Chung, T. D. *Anal. Chim. Acta* **2006**, *556*, 46.
(12) Jia, F.; Yu, C.; Deng, K.; Zhang, L. *J. Phys. Chem. C* **2007**, *111*, 8424.
(13) Jia, F.; Yu, C.; Ai, Z.; Zhang, L. *Chem. Mater.* **2007**, *19*, 3648.
(14) Song, Y. Y.; Zhang, D.; Gao, W.; Xia, X. H. *Chem.—Eur. J.* **2005**, *11*, 2177.
(15) Park, S.; Chung, T. D.; Kim, H. C. *Anal. Chem.* **2003**, *75*, 3046.
(16) Yuan, J. H.; Wang, K.; Xia, X. H. *Adv. Funct. Mater.* **2005**, *15*, 803.
(17) Chou, C. H.; Chen, J. C.; Tai, C. C.; Sun, I. W.; Zen, J. M. *Electroanalysis.* **2008**, *20*, 771.
(18) Hung, T.-K.; Lin, K.-W.; Tung, S.-P.; Cheng, T.-M.; Chang, I.-C.; Hsieh, Y.-Z.; Lee, C.-Y.; Chiu, H.-T. *J. Electroanal. Chem.* **2009**, *636*, 123.
(19) Chang, S. C.; Leung, L. W. H.; Weaver, M. J. *J. Phys. Chem.* **1990**, *94*, 6013.
(20) Ernst, S.; Heitbaum, J.; Hamann, C. H. *J. Electroanal. Chem.* **1979**, *100*, 173.
(21) Myung, Y.; Jang, D. M.; Cho, Y. J.; Kim, H. S.; Park, J.; Kim, J.-U.; Choi, Y.; Lee, C. J. *J. Phys. Chem. C* **2009**, *113*, 1251.
(22) Bikash Kumar, J.; Raj, C. R. *Chem.—Eur. J.* **2006**, *12*, 2702.
(23) Bai, Y.; Yang, W.; Sun, Y.; Sun, C. *Sens. Actuators, B* **2008**, *134*, 471.
(24) Zhou, Y.-G.; Yang, S.; Qian, Q.-Y.; Xia, X.-H. *Electrochem. Commun.* **2009**, *11*, 216.
(25) Li, Y.; Song, Y.-Y.; Yang, C.; Xia, X.-H. *Electrochem. Commun.* **2007**, *9*, 981.
(26) Zhao, W.; Xu, J.-J.; Shi, C.-G.; Chen, H.-Y. *Electrochem. Commun.* **2006**, *8*, 773.
(27) Wang, J.; Thomas, D. F.; Chen, A. *Anal. Chem.* **2008**, *80*, 997–1004.
(28) Hsiao, M. W.; Adzic, R. R.; Yeager, E. B. *J. Electrochem. Soc.* **1996**, *143*, 759.
(29) Popovic, K.; Tripkovic, A.; Markovic, N.; Adzic, R. R. *J. Electroanal. Chem.* **1990**, *295*, 79.
(30) Huang, T.-K.; Cheng, T.-H.; Yen, M.-Y.; Hsiao, W.-H.; Wang, L.-S.; Chen, F.-R.; Kai, J.-J.; Lee, C.-Y.; Chiu, H.-T. *Langmuir* **2007**, *23*, 5722.
(31) Huang, T.-K.; Chen, Y.-C.; Ko, H.-C.; Huang, H.-W.; Wang, C.-H.; Lin, H.-K.; Chen, F.-R.; Kai, J.-J.; Lee, C.-Y.; Chiu, H.-T. *Langmuir* **2008**, *24*, 5647.
(32) Chang, I.-C.; Huang, T.-K.; Lin, H.-K.; Tzeng, Y.-F.; Peng, C.-W.; Pan, F.-M.; Lee, C.-Y.; Chiu, H.-T. *ACS Appl. Mater. Interfaces* **2009**, *1*, 1375.
(33) Trasatti, S.; Petrii, O. A. *Pure Appl. Chem.* **1991**, *63*, 711.
(34) Sun, Y. P.; Buck, H.; Mallouk, T. E. *Anal. Chem.* **2003**, *73*, 1599.
(35) Cho, S.; Kang, C. *Electroanal.* **2007**, *19*, 2315.
(36) These electrochemical parameters can be found at the Web site: http://www.poc.roche.com/en_US/pdf/Evaluation_Report001.pdf.
(37) Rakhi, R. B.; Sethupathi, K.; Ramaprabhu, S. *J. Phys. Chem. B* **2009**, *113*, 3190.
(38) Hrapovic, S.; Liu, Y.; Male, K. B.; Luong, J. H. T. *Anal. Chem.* **2004**, *76*, 1083.

AM100432A